RESEARCH ARTICLE

Sustainable Hydrothermal Route for ZnO Nanoparticles using Berseem extract: A Structure–Property Correlation Study

Gurjinder Singh[1], **Vijay Kumar**[2], **Jyoti Gaur**[3,*] **and Sanjeev Kumar**[2,*]

[1] Department of Electrical and Electronics and Communication Engineering, DIT University, Dehradun 248009, India
[2] Department of Physics, Chandigarh University, Mohali 140413, India
[3] Bahra Research Innovation and Knowledge cluster, Rayat Bahra University, Mohali 140104, India

Abstract

This article explores the successful green synthesis of zinc oxide (ZnO) nanoparticles with a sustainable approach without using toxic chemicals or external stabilizers. The synthesized ZnO nanoparticles were characterized, and the investigation bridged the gap among physical, morphological, and optical properties. X-ray diffraction (XRD) analysis indicated the successful formation of a hexagonal wurtzite ZnO structure with an average crystallite size of 39.89 nm, representing high crystallinity and phase purity. The band gap energy was approximately 3.79 eV. UV-Visible results represented a strong optical absorption peak at 327 nm, proving the optical quality of the particles and exhibiting strong electronic transitions. Field-emission scanning electron microscopy (FESEM) results indicated the progression of rough agglomerated clusters into quasi-spherical well-dispersed particles through the growth process, while high-resolution transmission electron microscopy (HRTEM) images revealed uniformly sized particles of around 37 nm with a d-spacing of 2.60 Å between lattice fringes for further characterization. Meanwhile, the selected area electron diffraction (SAED) pattern obtained showed rings for polycrystalline ZnO representing the (100), (101), (102), (104), and (004) planes of the structure. Overall, the green-mediated synthesis approach resulted in high-purity and nanocrystalline ZnO particles with excellent structural and optical properties. The fabricated nanoparticles exhibit high potential for photocatalytic application, optoelectronic use, and UV-protective coatings; thus, efficiency suggests that a sustainable approach to fabrication allows for functionally efficient nanomaterials.

Keywords: green synthesis, optical properties, structural characterization, zinc oxide nanoparticles.

1 Introduction

Zinc oxide (ZnO) is one of the most favorable metal oxide semiconductors due to its direct band

Submitted: 05 October 2025
Accepted: 24 December 2025
Published: 30 December 2025

Vol. 1, **No.** 2, 2025.
10.62762/TAFMP.2025.399354

***Corresponding authors:**
✉ Jyoti Gaur
gaurj36@gmail.com
✉ Sanjeev Kumar
kumarsanju25@gmail.com

Citation
Singh, G., Kumar, V., Gaur, J., & Kumar, S. (2025). Sustainable Hydrothermal Route for ZnO Nanoparticles using Berseem extract: A Structure–Property Correlation Study. *ICCK Transactions on Advanced Functional Materials and Processing*, 1(2), 68–77.

© 2025 by the Authors. Published by Institute of Central Computation and Knowledge. This is an open access article under the CC BY license (https://creativecommons.org/licenses/by/4.0/).

gap of ∼3.37 eV and large exciton binding energy (∼60 meV), both of which enable efficient exciton production and retention at room temperature [1, 2]. Since quantum confinement effects are pronounced at the nano-level, ZnO also has a size-dependent band gap (3.20 to 3.45 eV) that can be precisely tuned via particle size (20–80 nm), making ZnO particularly useful for UV absorbing/photo responsive applications (e.g., photodetectors, UV-blocking paints) [3–5]. For example, ZnO nanoparticles (<40 nm) show increased photocatalytic degradation of methylene blue (MB) dye (>90% degradation in 60 min under 365 nm UV light at 10 mg/L dosage) as compared to bulk ZnO [6, 7]. The same is true for ZnO's antibacterial efficacy; ZnO nanoparticles exert bactericidal effects against E. coli and S. aureus more effectively than other sizes (35 nm mean diameter most effective at 25–50 µg/mL; >70 nm only ∼50% inhibition at >100 µg/mL) [8, 9]. ZnO is FDA GRAS approved (generally recognized as safe), making it viable for biomedical, food packaging, and cosmetic formulations, which is further complemented by the wide supply chain of zinc salts ($Zn(NO_3)_2{\cdot}6H_2O$/$Zn(CH_3COO)_2{\cdot}2H_2O$) from which it can be derived, including the high thermal stability (decomposition point of >1800°C) of ZnO lends itself well to industrial scale and economic feasibility. Thus, scientific publications documenting ZnO nanoparticles have increased approximately 400% in frequency from 2010 to 2022, demonstrating the strength of ZnO in nanoscience.

However, unfortunately for ZnO's vast potential, typical synthesis approaches, sol–gel, co-precipitation, hydrothermal, and chemical vapor deposition (CVD), tend to have serious shortcomings when controlling nanoparticle size, dispersion, surface chemistries, and crystallinities [10, 11]. For example, sol–gel methods tend to use surfactants or chelating agents (PVP, CTAB, EDTA), but these introduce unwanted organic remains that require calcination ≥500°C to remove [11]. Co-precipitation techniques generally provide wide size distributions (30–120nm) and stubborn agglomerates because of fast nucleation and Ostwald ripening. On the other hand, hydrothermal procedures more often yield with favorable crystallinity, but their processing time (12–24 h), processing temperature (up to 200 °C) [12], and use of autoclaves make such processes small-scale. Even more advanced techniques like CVD or spray pyrolysis need extremely pure precursors, vacuum applications, or flame combustion, which inflates energy use over 1.5kWh/g which shows that such processes cannot be low-cost or 'green' [13]. Furthermore, these processes generally lack repeatability; for example, pH, precursor concentration, and stir speed changes of 1 increment can result in ±20nm in crystallite size and ±0.1eV in optical band gap [14, 15]. Furthermore, higher dislocation densities ($\sim 1\times10^4$lines/m^2), microstrain values greater than 0.3% from conventional production methods can create a more disordered microstructure, which compromises structural integrity and decreases long-term stability of ZnO host materials. Finally, most of the conventional processes are not compatible with phytochemicals, which limit the ability to surface functionalize and maintain colloidal stability, which are prerequisites for bioengineering and optoelectronic applications.

Green synthesis of nanoparticles heralds a new era of sustainable nanotechnology where bioactive components found in plant-based solutions allow for the reduction, nucleation, growth, and stabilization of metal and metal oxide nanostructures. Unlike conventional chemistry routes that require hazardous reducing agents (e.g., sodium borohydride, hydrazine hydrate) and calcination steps >500°C to sinter particles, plant-mediated syntheses can occur in one-pot solutions through less aggressive aqueous environments (often <90–100°C) and neutral to alkaline pH (typical pH 8–11). The main benefit is derived from the multitude of phytocompounds within these biosolutions, including flavonoids, alkaloids, saponins, phenolics, tannins, and amino acids that act as dual agents to chelate Zn^{2+} ions while simultaneously directing the creation of ZnO nuclei through regulated hydrolysis and dehydration processes [16, 17]. For example, total phenolic content (TPC) has been reported to range from 2.5 to 6.0mg GAE/g across different studies to influence particle morphology and subsequent particles' surface energy and defect density observed in biosynthesized ZnO [18].

Controlled thermal treatment, generally at 300–450°C for 2–4 h, can subsequently remove excess organics while retaining nanoscale features; a variety of green synthesis studies document leaf extracts generating ZnO nanoparticles at such parameters with crystallite sizes of 20–50 nm, band gaps from 3.18 to 3.35 eV and BET surface areas of 30–60 m^2/g, no surfactant or capping agent needed. Furthermore, the volume of extract added and the molar ratios of extract to precursor are crucial; excess phytochemicals can generate excess capping and result in reduced grain growth as well as more organic residues, less means

not enough stabilization is present to prevent particle agglomeration. Ultimately, green-synthesized ZnO NPs recorded dislocation densities below 5×10^{13} lines/m^2 and microstrain values below 0.25%, which denote better crystallization and structure stability.

Mechanistically, biosynthesis can be simplified into three stages: (i) Zn^{2+} ions bind to hydroxyl or carbonyl functional groups in the extract; (ii) hydroxyl ions generated either from added NaOH or the basic nature of the extract result in hydrolysis to $Zn(OH)_2$; (iii) upon moderate heating, dehydration results in crystalline ZnO with size and morphology dependent upon the type and concentration of bioactive agents within the extract. Thus, the benefits of green synthesis involve eco-safety, cost savings, and scalability for a multitude of nanoparticles production with no need for after-synthesis isolation. Therefore, the green approach is the foundation of sustainable and functionally adjustable metal oxide nanomaterials. In parallel, plant-mediated green synthesis has been extensively explored for producing various metal oxide nanoparticles, including ZnO. Successful syntheses have been reported using diverse plant extracts such as *Aloe vera* for ZnO nanoparticles [19], *Terminalia arjuna* for CuO/rGO nanocomposites [20], various plants for copper nanoparticles [21], *Polystichum squarrosum* for ZnO nanoparticles [22], and various plants for rGO–ZrO_2 nanocomposites [24] demonstrating the versatility of this approach. The bioactive compounds in plant extracts act as reducing and stabilizing agents, governing nucleation and growth processes [23, 25]. However, the use of Trifolium alexandrinum (berseem) extract for ZnO synthesis remains unexplored, presenting an opportunity to utilize this regionally abundant, non-edible fodder crop for sustainable nanomaterial production.. Many plant species have been studied for nanoparticle biosynthesis, but *Trifolium alexandrinum*, or berseem, is one of the least utilized despite its phytochemically rich nature, extreme agricultural accessibility, and eco-regional relevance. Berseem is planted widely across the Indo-Gangetic plain; it is a legume that fixes nitrogen with a dry biomass yield of 15–20 tons/acre/year; thus, it is one of the most commercially important fodder crops in South Asia. More importantly, berseem leaves are biochemically active, containing ~14–18% protein, ~8–10% carbohydrates, and a high polyphenolic load (TPC ~3.1–4.5 mg GAE/g extract), which is comparable to or greater than that of commonly used synthesis matrices like *Azadirachta indica* or *Camellia sinensis* [26].

Such biochemical components are ideally suited to facilitate the green biosynthesis of ZnO nanoparticles. Many of the proteins and amino acids can take part as a soft template/capping agent via amino/carboxyl interactions. Similarly, some of the phenolics and flavonoids can reduce Zn^{2+} and modulate growth through metal–ligand chelation. Furthermore, berseem is neither edible nor cytotoxic, which means regional bioresource availability is not at risk by using a medicinal/edible plant as a source. Also, berseem is a seasonal crop, specific to the rabi cropping season, meaning this could facilitate lab-scale or semi-industrial nanoparticle production, as berseem could always be available through its own typical growth cycles. Most importantly, there have been NO peer-reviewed studies thus far noting *Trifolium alexandrinum* extract in the green biosynthesis of ZnO nanoparticles according to Scopus, Web of Science, and Google Scholar. Searches using "Trifolium alexandrinum" + "ZnO" and "Trifolium alexandrinum" + "ZnO" + "nanoparticle synthesis" yielded no results in reference to the green application of the plant extract, either. Thus, associated novelty in developing this source lies in its potential use within a structure-property tuning framework instead of a biological one, for such prospective use would be less novel. Thus, this work not only introduces a new phytochemical matrix to the world of green synthesis but also confirms this new, novel addition is capable of providing the desired characteristics (i.e., a mean crystallite size of around 40 nm, band gap tunability of ~3.22–3.30 eV, morphologically different particles) through a well-defined experimental process and correlating synthesized parameters relative to size-/defect-dependent structural features, confirming *Trifolium alexandrinum* as a bio-resource for sustainable materials science not previously tapped.

Recent plant-mediated syntheses of ZnO and other metal oxide nanoparticles have typically focused on extracts from medicinal or edible plants and have mainly emphasized biological activity or overall photocatalytic performance, with relatively limited attention to detailed structure-property correlations. In contrast, the present work introduces berseem, a non-edible fodder legume that is abundant in the Indo-Gangetic region, as a previously unexplored phytochemical matrix for ZnO and systematically links crystallite size, microstrain and optical band gap with the green hydrothermal synthesis conditions. This combination of a non-competitive agricultural bioresource and a structure-property-focused analysis

distinguishes our system from earlier plant-mediated ZnO reports.

The aim of this study is to provide a reproducible, green synthesis protocol for ZnO nanoparticles from *Trifolium alexandrinum* aqueous extract that can be biosynthesized with tunable physicochemical properties where a crystallite size of approximately 40 nm, tunable optical band gap from 3.20 to 3.30 eV and structural improvement is feasible and assessible in the laboratory using XRD, UV–Vis spectroscopy, FESEM and HRTEM for analysis relative to phase purity, morphology, and defect-related characteristics with systematic studies showing cause-and-effect relationship from green synthesis parameters compared to size-/defect-dependent structural descriptors.

2 Related Work

2.1 Materials

Zinc acetate dihydrate [$(CH_3COO)_2Zn{\cdot}2H_2O$; molecular weight: 219.50 g/mol; purity: 99.5%] was used as the zinc precursor for the green synthesis of ZnO nanoparticles. All chemicals employed in the study were of analytical grade and used without any further purification. Double-distilled (DD) water was used throughout all experimental processes to ensure purity and minimize ionic interference. Fresh leaves of *Trifolium alexandrinum* (commonly known as berseem) were collected from a local nursery in Kharar, Punjab, India. The collected plant material was authenticated based on morphological characteristics and used immediately for extract preparation.

2.2 Methodology

2.2.1 Phytochemical extraction via the Soxhlet method

About 300 g of fresh berseem (*Trifolium alexandrinum*) leaves were washed with warm double-distilled water (∼40 °C), shade-dried for 48 h and ground to a fine powder. The dried plant material was loaded into a Soxhlet extractor, and double-distilled water (1.5 L) was used as the extraction solvent. Extraction was carried out at gentle boiling for 6 h to allow repeated siphoning and efficient leaching of phytochemicals. The resulting aqueous extract was cooled to room temperature, filtered through Whatman No. 1 filter paper to remove residual solids and stored at 4 °C in amber bottles until further use.

2.2.2 Green synthesis of ZnO nanoparticles using Berseem extract

The precursor solution for zinc was obtained by weighing 19.75g of zinc acetate dihydrate ($(CH_3COO)_2Zn{\cdot}2H_2O$), the stoichiometric amount of Zn^{2+} ions needed and dissolving it into 50 mL of double-distilled water using magnetic stirring at room temperature for 15 minutes. Simultaneously, 400mL of fresh berseem aqueous extract was aliquoted in a clean beaker. The prepared zinc acetate precursor was added dropwise to the plant extract under mild stirring for uniform mixing and subsequent chelation, ensuring that bioactive agents from the plant could integrate with the Zn^{2+} ions. The mixture was stirred for an additional 10 minutes to allow Zn^{2+} ions chelation/reduction by phytochemicals from the berseem extract. The pH of the plant extract was determined to be 5.5 prior to the addition of the precursor, which increased to 6.0 after its addition. It has been established that a mildly alkaline pH favors the hydrolysis process with stabilization of $Zn(OH)_2$. Subsequently, ammonia solution (NH_4OH) was added dropwise to increase the pH to 9.0, determined with a digital pH meter. This adjustment favors nucleation and growth of ZnO nanoparticles. The solution was stirred for an additional 15 minutes to equilibrate the mixture before proceeding.

Then, the solution was transferred to a 1L Teflon-lined stainless-steel autoclave for hydrothermal synthesis wherein the autoclave was sealed tightly and placed in a hot air oven at 160°C for 17hours, benefitting from saturated pressure and thermal diffusion. At 17 hours, the autoclave was removed from the oven and allowed to cool down to room temperature (∼25°C) without restraint. Upon removal of the autoclave, a pale white precipitate is observed, confirming ZnO nanoparticle formation. To isolate the nanoparticles, the reaction mixture was subjected to centrifugation at 100,000 RPM for 12 minutes, and repeated three successive cycles to ensure maximum recovery and purity. The supernatant was discarded, and the collected pellet was washed with double-distilled water and then passed through Whatman No. 1 filter paper to eliminate residual phytochemicals and loosely bound ions. Finally, the filtered product was dried in a hot-air oven at 80°C for 5 hours, resulting in a dry, fine powder. This powder was gently ground using an agate mortar and pestle to obtain uniform, free-flowing ZnO nanoparticles, ready for structural and optical characterization.

2.3 Characterization Techniques

The synthesized ZnO nanoparticles were characterized to evaluate their structural, optical, and morphological properties. X-ray diffraction (XRD) was performed using a Bruker DB Advance diffractometer equipped

with Cu Kα radiation ($\lambda = 1.5406$ Å), operated at 40kV and 40mA. The scan was conducted in the 2θ range of 20° to 80°, and the resulting diffraction patterns were used to determine crystallinity and estimate average crystallite size using the Debye-Scherrer equation. The optical behavior of the ZnO nanoparticles was analyzed using a JASCO V-750 UV-Visible spectrophotometer in the wavelength range of 200–600nm. The sample was well-dispersed in distilled water, and the absorption spectra were recorded. The optical band gap energy was determined using the Tauc plot method, assuming a direct electronic transition $(\alpha h\nu)^2$ versus $h\nu$, as ZnO is a direct band gap semiconductor.

Surface morphology and particle distribution were observed using field emission scanning electron microscopy (FESEM) performed on a JEOL JSM-7610F Plus system. The powder was mounted on conductive tape, gold-coated, and imaged to examine particle shape, aggregation, and size distribution. Particle sizes were measured using ImageJ software. High-resolution transmission electron microscopy (HRTEM) was carried out using a JEOL JEM-2100 Plus microscope operated at 200 kV. Samples were dispersed in ethanol, dropped on carbon-coated copper grids, and dried before imaging. HRTEM provided lattice-resolved images and insight into nanoparticle shape and internal structure. Selected area electron diffraction (SAED) patterns were also recorded to confirm the crystalline nature.

3 Result and Discussion

3.1 XRD Analysis: Phase Purity and Crystallite Size Evaluation

X-ray diffraction (XRD) was performed to ascertain the crystalline structure and phase purity of the green-synthesized ZnO NPs. The XRD pattern obtained is shown in Figure 1(a) where the corresponding standard pattern for the hexagonal wurtzite ZnO (JCPDS 00-036-1451) is shown in Figure 1(b). The peaks at 2θ (Table 1) of 31.86°, 34.53°, 36.36°, 47.62°, 56.68°, 62.92°, 66.43°, 68.01°, 69.15° and 76.97°, respectively, are attributed to the (100), (002), (101), (102), (110), (103), (200), (112), (201), (004) and (202) planes, respectively. The presence of no peaks corresponding to impurities indicates high phase purity of the synthesized ZnO NPs. The observed sharp and well-defined diffraction peaks reveal good crystallinity, which is typical of hydrothermally synthesized ZnO. The average crystallite size (D) was deduced from the Debye-Scherrer equation:

$$D = \frac{K\lambda}{\beta \cos\theta} \tag{1}$$

where λ is the X-ray wavelength (1.5406 Å), β is the full width at half maximum (FWHM) in radians, θ is the Bragg angle, and K is the shape factor; thus, a value of $K = 0.9$ was taken into consideration. Calculated crystallite sizes were associated with certain planes ranging from 30.4 nm to 62.0 nm; for example, the (101) plane showed the greatest intensity in the obtained pattern with a crystallite size of approximately 44.4

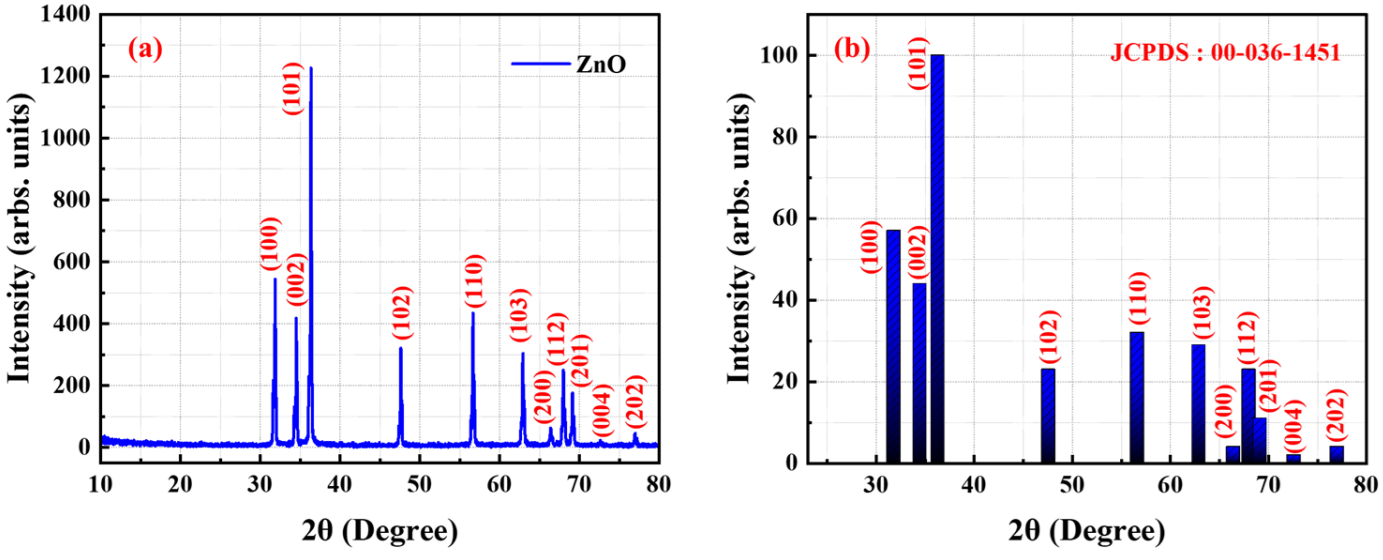


Figure 1. (a) XRD pattern of synthesized ZnO nanoparticles showing sharp peaks of wurtzite ZnO, (b) Standard reference confirming phase purity.

Table 1. XRD data of ZnO nanoparticles synthesized using Berseem extract, and Standard 2θ and d values.

2θ (Degree)	FWHM (β) (Degree)	Planes (hkl)	2θ (JCPDS 36-1451) (°)	2θ (JCPDS 36-1451) (Å)	Interplanar-spacing (d) (Å)	Crystallite size 'D' (nm)
31.865	0.1928	(100)	31.77	2.814	2.80	42.85
34.535	0.1872	(002)	34.42	2.603	2.59	44.44
36.360	0.17859	(101)	36.25	2.476	2.46	46.82
47.629	0.21724	(102)	47.54	1.911	1.90	39.97
56.677	0.26633	(110)	56.60	1.625	1.62	33.89
62.925	0.29114	(103)	62.86	1.477	1.47	31.99
66.425	0.28122	(200)	66.37	1.407	1.40	33.76
68.010	0.31485	(112)	67.96	1.378	1.37	30.43
69.145	0.30269	(201)	69.09	1.358	1.35	31.87
76.972	0.16141	(202)	76.98	1.238	1.23	62.87
						Average D=39.89 nm

nm, attributed to the dominant orientation of wurtzite ZnO's planes of symmetry. The average crystallite size was deduced to be approximately 39.89 nm, which closely resembles particle size on a nanoscale domain. Finally, the d-spacing values were calculated using Bragg's Law:

$$n\lambda = 2d\sin\theta \tag{2}$$

where $n = 1$, and comparable d-spacings were noted with the standard hexagonal ZnO phase. Of significance, the spacing for the (110) plane was calculated to be 1.62 Å, where the three most significant planes (100), (002), and (101) reveal d-spacings of approximately 2.80 Å, 2.59 Å, and 2.47 Å, respectively, suggesting proper crystalline formation and good definition of ZnO NPs. Thus, the XRD analysis confirms the successful formation of pure, crystalline ZnO nanoparticles with an average size close to 40 nm, a key design target of the study. The peak positions and intensities closely match the standard ZnO profile, and the narrow FWHM values reflect well-developed nanocrystallinity under optimized hydrothermal conditions.

3.2 Optical Properties and Band Gap Analysis of Green-Synthesized ZnO Nanoparticles

UV–Visible spectroscopy was then applied to assess the optical response and band structure of the synthesized ZnO nanoparticles. The absorption spectrum recorded (Figure 2) of biosynthesized ZnO nanoparticles between 200 and 600 nm reveals an intense, well-defined peak at 327 nm, a sign of the characteristic band-to-band transition from the O 2p valence band to that of the Zn 3d conduction band. Since the peak is relatively narrow and symmetric, it is indicative of good optical quality with even particle distribution without significant scattering due to defect-mediated phenomena; thus, it is a sign of successfully synthesized phase-pure ZnO nanocrystals.

Furthermore, the appearance of a single, absorbance tendency suggests nanoparticle dispersion and size homogeneity and strong electronic coupling between Zn and O orbitals. The observed absorption edge, slightly shifted to higher energies than previously reported for ZnO, suggests a slight blue shift due to quantum confinement phenomena as well as phonon coupling from the surface passivation by phytochemical capping agents from the plant extract. This bioactive component facilitates the reduction and stabilization of Zn^{2+} during the initiation of nucleation and particle growth, but at the same time, augments changes to surface electronic states by suppressing any oxygen-vacancy-linked defect transitions typically responsible for sub-bandgap absorption tailing. Ultimately, to calculate the optical band gap (E_g), the Tauc relation was applied.

$$(\alpha h\nu)^2 = A(h\nu - E_g) \tag{3}$$

where α is the absorption coefficient, $h\nu$ is the photon energy, and A is a proportionality constant. The plot of $(\alpha h\nu)$ versus $h\nu$, where the linear region was extrapolated, provided an optical band gap of 3.79 eV, confirming a direct allowed transition in ZnO. The slight widening of the optical band gap compared to standard values in microcrystalline form is attributed to particle size reduction, high surface energy, and

alteration in the local dielectric environment by organic surface components from the extract.

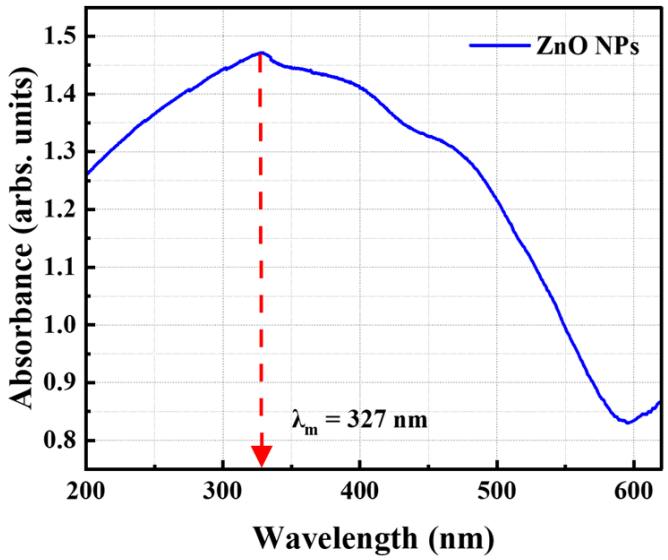


Figure 2. UV–Visible absorption spectrum of green-synthesized ZnO nanoparticles.

3.3 Surface Morphology Analysis via FESEM

Field emission scanning electron microscopy (FESEM) was used to assess the surface morphology and microstructure of the produced nanoparticles, as shown in Figure 3(a–d). The images compiled show the progression of ZnO nanostructured particles at various magnifications. At low and high powers, it confirms the creation of sub-micrometer particles with a rough, agglomerated surface morphology, characteristic of most bioassisted hydrothermal creations. At 20,000× magnification in Figure 3(a), 1 μm is the scale of measurement. One can see large secondary aggregates with nanosized crystallites densely packed within. Thus, these coarse clusters—and what appears to be a cauliflower-like morphology- generally occur when smaller primary particles fuse during the extended incubation time of hydrothermal treatment. These larger agglomerates develop an overview aspect of the bulk morphology and an indication of nucleation—growth facilitated by biochemicals in the green extract. At 30,000× (100 nm scale; Figure 3(b)), one can assess the surface granularity better. Here, the hierarchical structure seems apparent, comprised of fine nanoparticles—with many less than 100 nm—in addition to a textured base. The surface is uneven and rough in appearance, meaning that coalescence was not completed, in addition to natural stabilization from capping agents synthesized from the plant extract. The presence of these features implies that the pathway generally assessed during green synthesis favored particle agglomeration and surface-dependent nucleation over growth free from particles.

At 50,000× magnification, quasi-spherical and sub-angular nanoparticles can be distinguished. Figure 3(c) implies that homogeneity exists at lower resolution across the surface with variable sizes and boundaries for many particles. Thus, agglomeration was limited by the appealing characteristics imparted by organic ligands derived from the extract of berseem components. These high-resolution perspectives are consistent with XRD results pertaining to crystalline sizes (∼30-62 nm), indicating small nanometrics consistent with a nanometric system. Finally, in Figure 3(d) at 100,000×, high-resolution imaging can better visualize subtle distinctions of surface topology as one notes differentiation among distinct nanograins on top of possibly smoother, sheet-like structures below. The appearance of some hexagonal or faceted particles suggests partial shape development under the influence of controlled hydrothermal crystallization. The underlying matrix appears less porous, indicating that nucleation likely occurred over a condensed organic or crystalline base formed during early stages of synthesis. Together, the FESEM images affirm that the synthesized ZnO nanoparticles are highly crystalline, nanoscale, and morphologically diverse, with particle sizes consistent with XRD findings. The observed morphology, ranging from rough agglomerated clusters to well-dispersed quasi-spherical particles, demonstrates the role of the berseem extract in modulating nucleation, growth, and aggregation behaviors during the green hydrothermal process.

3.4 High-Resolution Transmission Electron Microscopy (HRTEM): Size, Lattice, and Crystallinity Confirmation

High-resolution transmission electron microscopy (HRTEM) was used to analyze the internal structure, particle morphology, and lattice attributes of the biosynthesized ZnO nanoparticles. Figure 4(a–d) shows representative HRTEM images taken at various levels of magnification, where indirect measurements manifest direct evidence concerning particle size and lattice arrangement as well as polycrystallinity.

For example, Figure 4(a) shows multiple nanoparticles with distinguishable boundaries and edges that have been measured to be sized in the ∼29.5 to 46.5 nm spectrum. This finding confirms a well-distributed nanoparticle population as previously detected

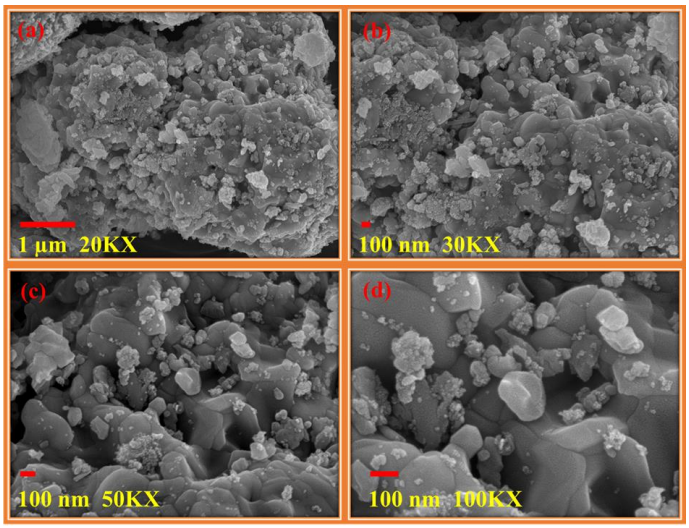


Figure 3. FESEM micrographs of ZnO nanoparticles synthesized using *Trifolium alexandrinum* extract at different magnifications: (a) 20,000× (scale bar = 1 μm), (b) 30,000× (scale bar = 100 nm), (c) 50,000× (scale bar = 100 nm) and (d) 100,000× (scale bar = 100 nm).

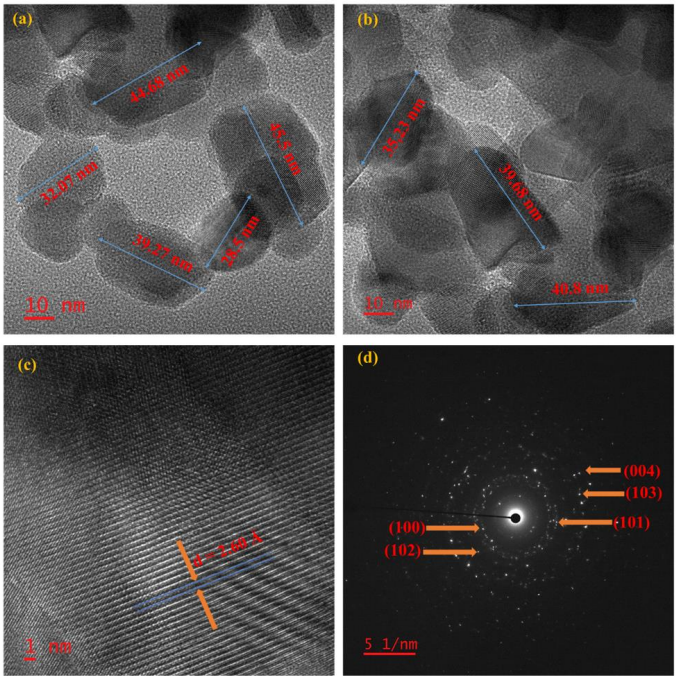


Figure 4. HRTEM images and SAED pattern of green-synthesized ZnO nanoparticles: (a, b) low- and high-magnification images (scale bars as shown) of well-dispersed particles; (c) lattice fringes with interplanar spacing ≈ 0.26 nm indexed to a ZnO plane; (d) SAED pattern showing rings indexed to the hexagonal wurtzite structure.

under FESEM measurements. Furthermore, these particles exhibit quasi-spherical to quasi-elongated morphologies, consistent with the expected natural growth tendencies of ZnO when produced at elevated temperatures and under hydrothermal conditions. Figure 4(b) shows a similarly distributed size area and inclusion size in the range of ∼35.2 and 40.8 nm with a very visible lattice. It's noted that the average particle size from HRTEM reports taken over several instances is estimated to be about 37 nm, corresponding with XRD (XRD average is assessed at ∼39.9 nm) and FESEM results (FESEM determined an average of ∼30–60 nm).

Figure 4(c) demonstrates an up-close lattice-resolved picture of one ZnO nanoparticle, which exhibits clear and continuous lattice fringes. This suggests a high degree of crystallinity in the observed fragment. The interplanar distance measured is ∼2.60 Å, correlating to the (002) plane of the hexagonal wurtzite structure of ZnO, confirming that plant-extract mediated synthesis produces a naturally ordered crystalline arrangement with significance of periodicity on the inside. Finally, Figure 4(d) displays the selected area electron diffraction (SAED) pattern recorded from the sample, showing a diffused ring pattern superimposed with formal spots of diffraction, characteristic of polycrystalline nanomaterials. Each of the rings relates to the (100), (101), (102), (103), and (004) planes of hexagonal ZnO in close correspondence to the standard wurtzite ZnO diffraction indices given. In addition, the clear spots and rings separated suggest high levels of crystallinity and phase purity, while the spotty nature suggests larger sizes of coherent domains that can diffract.

Overall, the HRTEM analysis confirms the successful formation of uniform, crystalline ZnO nanoparticles with an average size of ∼37 nm. The combination of well-resolved lattice fringes and indexed SAED patterns verifies the high structural order and polycrystalline nature of the ZnO system, reflecting the effectiveness of the *Trifolium alexandrinum*-mediated green hydrothermal synthesis route in controlling particle size and crystallinity.

4 Conclusion

In summary, green synthesis of ZnO nanoparticles was successfully achieved using a simple, eco-friendly route that yielded highly crystalline and phase-pure ZnO nanostructures. The XRD analysis confirmed the formation of a single-phase hexagonal wurtzite ZnO structure without any secondary impurities, exhibiting an average crystallite size of 39.89 nm, indicative of well-developed nanocrystals. The UV–Visible spectral study revealed a sharp and intense absorption peak at 327 nm, corresponding to a direct optical band gap

of 3.79 eV calculated via Tauc's relation. This wide band gap and strong UV absorption highlight the semiconducting nature and optical transparency of the synthesized material, suitable for photoactive and optoelectronic applications.

The FESEM micrographs displayed a morphological transition from rough, agglomerated clusters to well-dispersed quasi-spherical nanoparticles, suggesting that the green synthesis approach effectively controlled surface growth and prevented severe agglomeration. These observations were further validated by HRTEM, which revealed distinct lattice fringes with an interplanar d-spacing of 2.60 Å, corresponding to the (100) plane of wurtzite ZnO, and an average particle size of ∼37 nm, in excellent agreement with the XRD results. The accompanying SAED pattern exhibited well-defined concentric diffraction rings indexed to the (100), (101), (102), (104), and (004) planes, confirming the polycrystalline and defect-free nature of the nanoparticles.

Collectively, these results affirm that the adopted green synthesis route is an effective, sustainable, and reproducible method for producing high-purity, nanocrystalline ZnO particles with superior structural integrity and favorable optical properties. Such well-crystallized and optically active ZnO nanoparticles hold strong potential for applications in photocatalysis, UV-shielding materials, biosensing, and optoelectronic devices, where surface activity, band-gap precision, and structural stability are of critical importance.

Data Availability Statement

Data will be made available on request.

Funding

This work was supported without any funding.

Conflicts of Interest

The authors declare no conflicts of interest.

Ethical Approval and Consent to Participate

Not applicable.

References

[1] Sharma, D. K., Shukla, S., Sharma, K. K., & Kumar, V. (2022). A review on ZnO: Fundamental properties and applications. *Materials Today: Proceedings, 49*, 3028-3035. [Crossref]

[2] Özgür, Ü., Alivov, Y. I., Liu, C., Teke, A., Reshchikov, M. A., Doğan, S., ... & Morkoç, A. H. (2005). A comprehensive review of ZnO materials and devices. *Journal of applied physics, 98*(4). [Crossref]

[3] Khairnar, N., Kwon, H., Park, S., Lee, H., & Park, J. (2023). Tailoring the size and shape of ZnO nanoparticles for enhanced performance of OLED device. *Nanomaterials, 13*(21), 2816. [Crossref]

[4] Gu, Y., Kuskovsky, I. L., Yin, M., O'brien, S., & Neumark, G. F. (2004). Quantum confinement in ZnO nanorods. *Applied physics letters, 85*(17), 3833-3835. [Crossref]

[5] Liu, K., Sakurai, M., & Aono, M. (2010). ZnO-based ultraviolet photodetectors. *Sensors, 10*(9), 8604-8634. [Crossref]

[6] Atta, D., Wahab, H. A., Ibrahim, M. A., & Battisha, I. K. (2024). Photocatalytic degradation of methylene blue dye by ZnO nanoparticle thin films, using Sol–gel technique and UV laser irradiation. *Scientific Reports, 14*(1), 26961. [Crossref]

[7] Isai, K. A., & Shrivastava, V. S. (2019). Photocatalytic degradation of methylene blue using ZnO and 2% Fe–ZnO semiconductor nanomaterials synthesized by sol–gel method: a comparative study. *SN Applied Sciences, 1*(10), 1247. [Crossref]

[8] El-Fallal, A. A., Elfayoumy, R. A., & El-Zahed, M. M. (2023). Antibacterial activity of biosynthesized zinc oxide nanoparticles using Kombucha extract. *SN Applied Sciences, 5*(12), 332. [Crossref]

[9] Raghupathi, K. R., Koodali, R. T., & Manna, A. C. (2011). Size-dependent bacterial growth inhibition and mechanism of antibacterial activity of zinc oxide nanoparticles. *Langmuir, 27*(7), 4020-4028. [Crossref]

[10] Zhou, X. Q., Hayat, Z., Zhang, D. D., Li, M. Y., Hu, S., Wu, Q., ... & Yuan, Y. (2023). Zinc oxide nanoparticles: synthesis, characterization, modification, and applications in food and agriculture. *Processes, 11*(4), 1193. [Crossref]

[11] Dey, S., lochan Mohanty, D., Divya, N., Bakshi, V., Mohanty, A., Rath, D., ... & Sabui, R. (2025). A critical review on zinc oxide nanoparticles: Synthesis, properties and biomedical applications. *Intelligent Pharmacy, 3*(1), 53-70. [Crossref]

[12] Mishra, S., Paszkowicz, W., Sulich, A., Jakiela, R., Ożga, M., & Guziewicz, E. (2022). Electrical and Structural Properties of Semi-Polar-ZnO/a-Al2O3 and Polar-ZnO/c-Al2O3 Films: A Comparative Study. *Materials, 16*(1), 151. [Crossref]

[13] Podrezova, L. V., Porro, S., Cauda, V., Fontana, M., & Cicero, G. (2013). Comparison between ZnO nanowires grown by chemical vapor deposition and hydrothermal synthesis. *Applied Physics A, 113*(3), 623-632. [Crossref]

[14] Prabhu, Y. T., Rao, K. V., Kumar, V. S. S., & Kumari, B. S. (2014). X-ray analysis by Williamson-Hall and size-strain plot methods of ZnO nanoparticles with

fuel variation. *World Journal of Nano Science and Engineering, 2014*. [Crossref]

[15] Sharma, V., Sharma, J. K., Kansay, V., Sharma, V. D., Sharma, A., Kumar, S., ... & Bera, M. K. (2023). The effect of calcination temperatures on the structural and optical properties of zinc oxide nanoparticles and their influence on the photocatalytic degradation of leather dye. *Chemical Physics Impact*, *6*, 100196. [Crossref]

[16] Alharbi, F. N., Abaker, Z. M., & Makawi, S. Z. A. (2023). Phytochemical substances—mediated synthesis of zinc oxide nanoparticles (ZnO NPS). *Inorganics*, *11*(8), 328. [Crossref]

[17] Mutukwa, D., Taziwa, R., & Khotseng, L. E. (2022). A review of the green synthesis of ZnO nanoparticles utilising Southern African indigenous medicinal plants. *Nanomaterials*, *12*(19), 3456. [Crossref]

[18] Rodríguez-Barajas, N., Ponce-Regalado, M. D., Segura-Almendárez, M. S., Rodríguez-Razon, C. M., Ghotekar, S., Fellah, M., & Pérez-Larios, A. (2024). Plant-mediated synthesis and interaction of ZnO against breast and prostate cancer. *Results in Chemistry*, *9*, 101654. [Crossref]

[19] Sangeetha, G., Rajeshwari, S., & Venckatesh, R. (2011). Green synthesis of zinc oxide nanoparticles by aloe barbadensis miller leaf extract: Structure and optical properties. *Materials Research Bulletin*, *46*(12), 2560-2566. [Crossref]

[20] Kumari, V., Kaushal, S., & Singh, P. P. (2022). Green synthesis of a CuO/rGO nanocomposite using a Terminalia arjuna bark extract and its catalytic activity for the purification of water. *Materials Advances*, *3*(4), 2170-2184. [Crossref]

[21] Nieto-Maldonado, A., Bustos-Guadarrama, S., Espinoza-Gomez, H., Flores-López, L. Z., Ramirez-Acosta, K., Alonso-Nuñez, G., & Cadena-Nava, R. D. (2022). Green synthesis of copper nanoparticles using different plant extracts and their antibacterial activity. *Journal of Environmental Chemical Engineering*, *10*(2), 107130. [Crossref]

[22] Sodhi, R. S., Singh, P. P., Lal, B., Joshi, S. K., Kumar, R., Singh, Y., & Kaushal, S. (2024). Biogenic synthesis of ZnO nanoparticles using Polystichum squarrosum extract and its applications as anti-oxidant, anti-diabetic agent and industrial waste water treatment. *Emergent Materials*, *7*(1), 285-298. [Crossref]

[23] Mittal, A. K., Chisti, Y., & Banerjee, U. C. (2013). Synthesis of metallic nanoparticles using plant extracts. *Biotechnology advances*, *31*(2), 346-356. [Crossref]

[24] Kaushal, S., Kumari, V., & Singh, P. P. (2023). Sunlight-driven photocatalytic degradation of ciprofloxacin and organic dyes by biosynthesized rGO–ZrO2 nanocomposites. *Environmental Science and Pollution Research*, *30*(24), 65602-65617. [Crossref]

[25] Iravani, S. (2011). Green synthesis of metal nanoparticles using plants. *Green Chemistry*, *13*(10), 2638-2650. [Crossref]

[26] Tava, A., Pecio, Ł., Lo Scalzo, R., Stochmal, A., & Pecetti, L. (2019). Phenolic content and antioxidant activity in Trifolium germplasm from different environments. *Molecules*, *24*(2), 298. [Crossref]



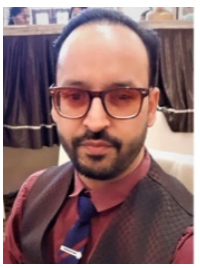
Dr. Gurjinder Singh is an Associate Professor in the Department of Electrical & Electronics & Communication Engineering at DIT University, Dehradun, having joined in July 2023. He holds a Ph.D. in ECE from Desh Bhagat University and an M.Tech from Panjab University. With nearly two decades of experience in teaching, research, and industry, his specialization lies in nanoelectronics and the optical and electronic properties of metal-oxide semiconductor nanomaterials. His research spans chemical and green synthesis methods, photoluminescence, photocatalysis, and device applications. He teaches courses such as Analog Integrated Circuits, Nanoelectronics, and Optical Fiber Communication. (Email: gurjindersingh@yahoo.com)



Vijay Kumar is an M.Sc. Physics student at Chandigarh University, India. His research focuses on the green synthesis and characterization of metal oxide nanoparticles using plant extracts for environmental and biomedical applications. He is particularly interested in developing nanotechnology-based sustainable approaches to address real-world challenges. (Email: whoovijay@gmail.com)



Dr. Jyoti Gaur is a Research Assistant Professor at Rayat Bahra University, working in the Research & Innovation Cell. Her research focuses on the green synthesis of metal-oxide nanomaterials for environmental and photocatalytic applications. She is associated with the Research Laboratory of 3D Bioprinting Technologies for Flexible Electronics, Southern Federal University, Russia, for prospective postdoctoral research. (Email: gaurj36@gmail.com)



Dr. Sanjeev Kumar is Associate Professor of Physics at Chandigarh University, Mohali, where his research focuses on experimental condensed matter physics, especially superconductivity and magnetism in bulk and low-dimensional materials. He earned his M.Sc. in Electronics (as a gold medalist) and Ph.D. in Materials Science. Over his career, he has published more than 100 research papers, 4 patents and works on novel materials and electronic phenomena at low temperatures. He collaborates broadly and has developed synthesis protocols for diverse nanostructures applied to fields like gas sensing, catalysis and electronics. (Email: Kumarsanju25@gmail.com)